Reddy *et al.*
Journal of Analytical Science and Technology (2024) 15:53
https://doi.org/10.1186/s40543-024-00466-w

Journal of Analytical Science and Technology

RESEARCH ARTICLE Open Access

Electrochemical nucleation and growth model of MoS_2 for hydrogen evolution reaction

Venumbaka Maneesh Reddy[1], Marepally Bhanu Chandra[2], Saravanan Gengan[3*] and Selvakumar Duraisamy[1*]

Abstract

The electrochemical nucleation of MoS_2 from a mixture of sodium molybdate dihydrate ($Na_2MoO_4{\cdot}2H_2O$) and sodium sulphide ($Na_2S{\cdot}xH_2O$) aqueous solution on Cu substrate has been investigated. The nucleation and formation of molybdenum sulphide were investigated employing cyclic voltammetry and chronoamperometry studies. The experimental i–t curves observed at various overpotentials were compared to theoretical curves derived for the two limiting situations of the 3D instantaneous/progressive nucleation and growth model, as reported by Scharifker and Hills. The outcome of electrodeposition potential on nucleation rate (A) and nucleation density (N) was calculated from the current–time transients and SEM morphology obtained at − 1.1 V (5.75×10^{14} and 1.86×10^{15}) was compared with − 0.9 V, − 1.0 V, and − 1.2 V, respectively. The investigation of the initial stages of the transient current–time relationships developed for MoS_2 electrodeposition specified that film formation occurred progressively initially and instantaneous nucleation during the course of time. A HPMoS_2 with an average size of 5–65 nm was obtained at -1.1 V and exhibited superior performance towards the hydrogen evolution reaction compared to samples obtained at − 0.9 V, − 1.0 V, and − 1.2 V.

Introduction

Molybdenum disulphide (MoS_2), a member of the layered transition metal dichalcogenides (TMDCs), has emerged as a promising material for various electronic and optoelectronic applications due to its exceptional physical and chemical properties. TMDCs like MoS_2 have a unique structure, composed of layers of molybdenum (Mo) atoms sandwiched between sulphur (S) atoms, forming a stable S-Mo-S coordination within the crystal lattice. This layered structure allows for intriguing electrical, mechanical, and chemical characteristics, such as a tuneable band gap, making MoS_2 suitable for a range of semiconductor applications including transistors, photodetectors, and flexible electronics (Mak et al. 2010; Splendiani et al. 2010; Radisavljevic et al. 2011). One of the key advantages of MoS_2 is its abundance and low-cost production, which, combined with its adjustable band gap, enables the development of highly efficient switchable transistors. The band gap of MoS_2 can be modulated based on the number of layers, ranging from an indirect band gap (~1.2 eV) in bulk form to a direct band gap (~1.8 eV) in monolayers. This transition from bulk to monolayer introduces unique optical and electronic properties, which are significantly different from those observed in bulk materials. Such properties have positioned MoS_2 as a leading candidate for next-generation optoelectronic devices, including photodetectors, solar cells, and light-emitting diodes (Lembke and Kis 2012; Yin et al. 2012; Shi et al. 2012). In addition to its

*Correspondence:
Saravanan Gengan
saravanan3che@gmail.com
Selvakumar Duraisamy
selvakumar@psgitech.ac.in
[1] Department of ECE, PSG Institute of Technology and Applied Research, Coimbatore 641062, India
[2] Chaitanya Bharati Institute of Technology, Hyderabad, Telangana 500075, India
[3] Department of Chemistry, Saveetha School of Engineering, Saveetha Institute of Medical and Technical Sciences, Saveetha University, Chennai, Tamil Nadu 602105, India

electronic applications, MoS_2 exhibits excellent catalytic properties, particularly in photocatalytic and electrocatalytic reactions. The presence of unsaturated molybdenum and sulphur atoms at the edges of the material's crystal lattice creates active sites that facilitate hydrogen production through water splitting. These active sites, resulting from the S-Mo-S coordination, enhance the material's catalytic efficiency, making MoS_2 an attractive material for hydrogen evolution reactions (HER). Its high surface area and catalytic activity, combined with its stability in aqueous environments, further emphasize its potential in renewable energy technologies (Voiry et al. 2016; Yu et al. 2014; Novoselov et al. 2005).

To exploit the properties of MoS_2 for various applications, several fabrication methods have been developed. Top-down techniques, such as micromechanical exfoliation, intercalation-assisted exfoliation, and liquid-phase exfoliation, are widely used to isolate monolayers or few-layer MoS_2 from bulk crystals. These methods, while effective in producing high-quality monolayers, face limitations in terms of scalability and cost for industrial-scale production. Alternatively, bottom-up approaches like physical vapour deposition (PVD), chemical vapour deposition (CVD), and atomic layer deposition (ALD) provide better control over the growth and thickness of MoS_2 films, but these methods can be expensive and challenging to implement on a large scale (Zeng et al. 2017; Li et al. 2014; Yu et al. 2013). Electrochemical deposition (or electrodeposition) offers a cost-effective and scalable alternative for producing MoS_2 thin films and nanoparticles under ambient conditions. This method allows for precise control over critical deposition parameters such as film thickness, particle size, and morphology, making it suitable for large-scale manufacturing. Additionally, electrodeposition occurs under room temperature and pressure conditions, eliminating the need for complex equipment or toxic chemical reducing agents, further enhancing its industrial viability. Recent studies have successfully demonstrated the electrodeposition of MoS_2 onto various substrates, providing insights into the material's nucleation and growth mechanisms (Kong et al. 2014; Alinejadian et al. 2022; Zhou et al. 2013). Despite these advancements, the nucleation and growth dynamics of MoS_2 during electrodeposition remain relatively unexplored. Understanding these mechanisms is crucial for optimizing the electrodeposition process to achieve desired material properties. This study investigates the electrodeposition of MoS_2 at different overpotentials ranging from -0.9 to -1.2 V, using sodium molybdate dihydrate and sodium sulphide as precursors in a potentiostatic, charge-controlled deposition process. By comparing theoretical nucleation models with experimental observations, this research aims to elucidate the electrochemical behaviour of MoS_2 during deposition. Scanning electron microscopy (SEM) is employed to characterize the morphology of the deposited MoS_2 films, providing insights into how deposition conditions influence the material's structure and properties. This investigation highlights the potential of electrodeposition as a scalable and cost-effective method for fabricating MoS_2 with tunable properties. By operating under room temperature and pressure, and without the need for hazardous chemicals, this technique offers a promising route for the sustainable production of MoS_2 for various industrial applications (Tan and Zhang 2015; Du et al. 2014; Singh et al. 2023; Aslan et al. 2021).

Experimental

Electrochemical preparation of MoS_2 nanostructures on Cu substrate

To investigate the electrochemical phase formation of MoS_2 nanostructures on a Cu substrate, we prepared an electrolyte mixture consisting of 1 M $Na_2MoO_4{\cdot}2H_2O$ and 0.1 M $Na_2S{\cdot}xH_2O$ dissolved in 20 ml of Milli-Q water. This mixture was magnetically stirred for 30 min and maintained at 65–70 °C. Following that, the electrodeposition of MoS_2 took place within a three-electrode cell arrangement, with Cu foils serving as the working electrode (WE), Pt mesh electrode as the counter electrode (CE), and a saturated KCl–Ag/AgCl reference electrode (RE). Constant applied (CA) curves were employed for electrodeposition potentials of -0.9 V, -1.0 V, -1.1 V, and -1.2 V, respectively, for a duration of 200 s, as depicted in Scheme 1. The resulting samples were designated as $FNMoS_2$, $SSMoS_2$, $HPMoS_2$, and $LPMoS_2$, corresponding to the applied potentials. Following electrodeposition, the Cu electrodes with MoS_2 were cleaned using deionized (DD) water to remove any residual electrolyte. To improve adhesion, a drop of a 1:1 mixture of Nafion and ethanol was spread onto the deposited MoS_2, and the electrodes were then allowed to dry overnight at room temperature.

Electrochemical characterization and surface morphology studies

Electrochemical analysis was conducted using a Princeton Applied Research Model PARSTAT 2273 potentiostat–galvanostat, which was controlled by Power Suite software. The experiments utilized a conventional three-electrode electrochemical cell setup. The working electrode consisted of a platinum wire with a surface area of 0.15 cm^2. These investigations involved potential step cyclic voltammetry, a technique where a series of potential steps are applied to the working electrode to measure resulting currents. This methodology provides valuable insights into the electrochemical behaviour of the system

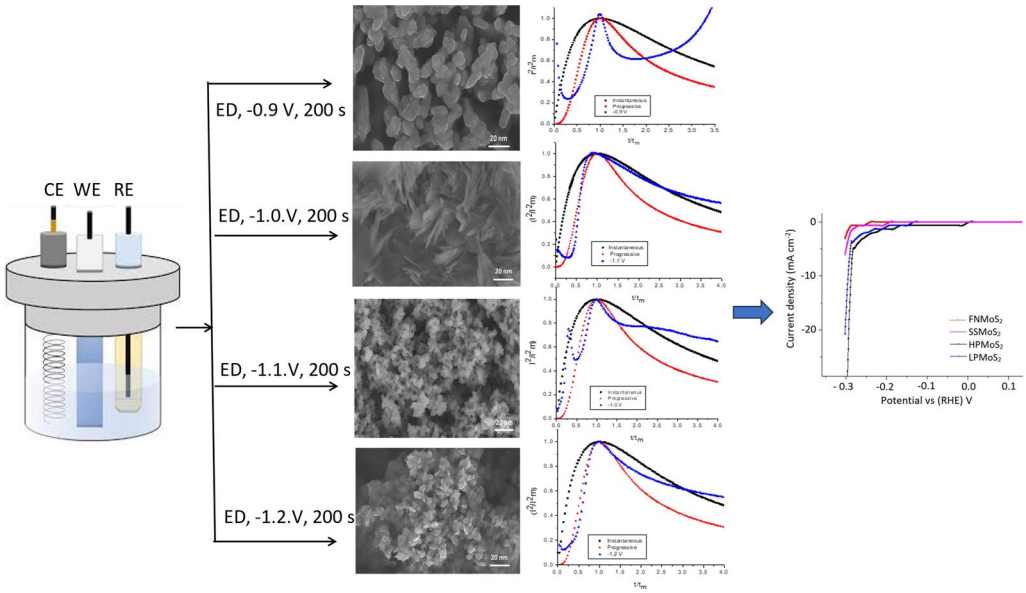

Scheme 1 Schematic illustration of the electrochemical phase formation of MoS_2 at −0.9 V, −1.0 V, −1.1 V, and −1.2 V, respectively, corresponding SEM images and its dimensionless time vs. dimensionless current instantaneous and progressive nucleation model in mixture ($Na_2MoO_4.2H_2O$ and $Na_2S.XH_2O$) electrolyte solution

under study, including redox reaction kinetics, surface adsorption processes, and the formation of reaction intermediates. A saturated Ag/AgCl electrode equipped with a Luggin capillary served as the reference electrode, while a platinum sheet acted as the counter electrode. Throughout the experiments, all potentials were applied at values of −0.9 V, −1.0 V, −1.1 V, and −1.2 V, respectively. These potentials were maintained for a duration of 200 s in a solution containing $Na_2MoO_4{\cdot}2H_2O$ and $Na_2S{\cdot}xH_2O$.

Results and discussion

Cyclic voltammetry investigation of formation of MoS_2

In our experiments, tetra thiomolybdate was formed by simply mixing Na_2MoO_4 and Na_2S in Milli-Q water to investigate the formation of MoS_2 through cyclic voltammetry (CV). The CV results revealed a distinct pattern of MoS_3 formation and dissolution, as depicted in Fig. 1. Specifically, MoS_3 film formation was observed through the oxidation of $[MoS_4]^{2-}$ ions at −0.625 V, followed by its dissolution upon reduction at + 0.3 V. This observation is consistent with previous literature reports (Shi et al. 2015), suggesting that MoS_3 is generated via the following processes: process (1) oxidation: $[MoS_4]^{2-} \rightarrow MoS_3 + S^{2-}$—(1), reduction: $MoS_3 \rightarrow MoS_4{}^{2-}$—(2) however, it is important to note that the reduction of MoS3 to form $MoS_4{}^{2-}$ is also possible, potentially due to the reverse reaction of Eq. 1. It is crucial to recognize that both equations are not entirely

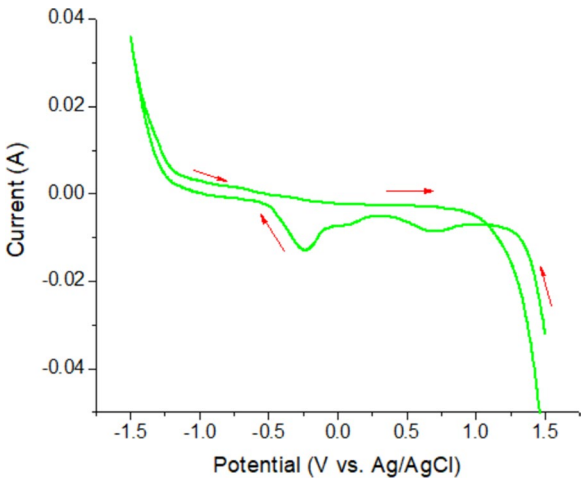

Fig. 1 CV curve recorded in the solution of $Na_2MoO_4.2H_2O$ and $Na_2S.XH_2O$ in 20 ml of Milli-Q water over the range of − 1.5 to + 1.5 V at scan rate of 5 mV/s

reversible, implying that the comparative rates of electrodeposition and dissolution can be influenced by different electrodeposition parameters. Furthermore, during the negative-going scan at -0.25 V, a reductive deposition is observed. This process can be attributed to the following reaction, consistent with previously reported literature: reductive deposition: Formation of MoS_2 possibly combined through MoS_3 in the film. Moreover, it is worth considering that OH^- and hydrosulphide may mix with

molybdenum during these processes, and these negative groups could potentially undergo additional transformations into numerous O^{2-} and S^{2-} species. For instance, the cyclic voltammetry study reveals a dynamic process of MoS_3 formation and its subsequent dissolution, as well as the possible formation of amorphous MoS_2. These observations underscore the complexity of the electrochemical nature of MoS_2 and the importance of controlling deposition conditions to tailor the properties of the resulting material.

$$[MoS_4]^{2-} \rightarrow MoS_3 + 1/8\ S_8 + 2e^- \quad (1)$$

$$MoS_3 + 1/8\ S_8 + 2e^- \rightarrow [MoS_4]^{2-} \quad (2)$$

$$[MoS_4]^{2-} + 2H_2O + 2e^- \rightarrow MoS_2 + 2SH^- + 2OH^- \quad (3)$$

Electrochemical study of MoS_2 deposition by the chronoamperometric method

To investigate the specific reactions involved in nucleation and growth, chronoamperometric analysis (CA) was employed. CA curves were examined over a potential range from −0.9 to −1.2 V. Figure 2 displays typical fluctuations in current density. Figure 2 shows that the current quickly rises to its maximum value (i_{max} at t_{max}) before gradually declining over time. The abrupt increase in current in the cathodic direction can be attributed to either an augmentation in the number of nuclei or the emergence of a new phase. During the development of the deposit, nuclei generate diffusion zones around themselves. These zones impede hemispherical mass transfer and facilitate linear mass transfer, resulting in a predominantly flat surface. As the current diminishes due to linear diffusion control, as elucidated by the Cottrell equation, the thickness of the diffusion layer increases (Saravanan and Mohan 2016).

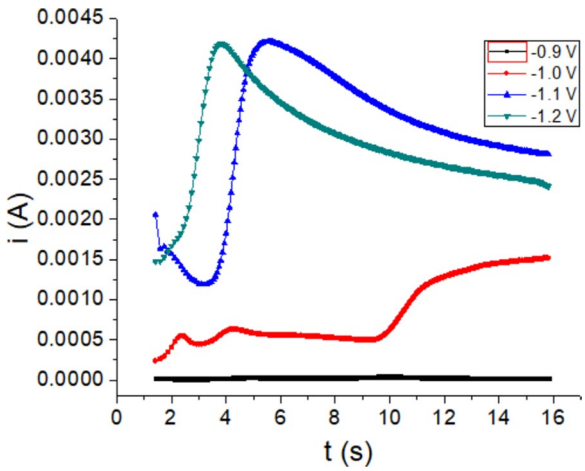

Fig. 2 CA of $FNMoS_2$/Cu, $SSMoS_2$/Cu, $HPMoS_2$/Cu, and $LPMoS_2$/Cu electrochemical phase formation at −0.9 V, −1.0 V, −1.1 V, and −1.2 V for 200 s, respectively

3D instantaneous/progressive nucleation and growth model

Analysing the generated CA curves using equations from the Scharifker–Hills (SH) model can provide insight into the process of nucleation and crystal development, allowing for comparison with acquired data (Cottrell 1903; Scharifer and Hills 1983). According to the proposed model, nucleation processes are categorized into two types: instantaneous and progressive. The instantaneous type entails nucleus development occurring immediately upon the application of the deposition potential. In contrast, progressive nucleation involves the continual proliferation of nuclei during the electrochemical deposition experiment. These two assumptions for instantaneous and gradual nucleation can be expressed as Eqs. (4) and (5).

$$i^2/i_m^2 = 1.9542/(t/t_m)\{1 - \exp[-1.2564(t/t_m)]\}^2 \quad (4)$$

$$i^2/i_m^2 = 1.2254/(t/t_m)\left\{1 - \exp\left[-2.3367(t/t_m)^2\right]\right\}^2 \quad (5)$$

The mathematical study of the nucleation model in the electrolyte solution at different potentials was performed using SH equations (Gunawardena et al. 1982). However, it was discovered that the resultant currents at constant potentials are not always constant, since they are impacted by numerous factors: (1) The nucleation and growth mechanisms of MoS_2 are time and overpotential dependent. (2) The existence of faulty patches and the electrode's surface roughness can help define the usual nucleation and growth mechanisms. These features can make it challenging to explain the deposition behaviour of 3D tiny nodular grains, small sheetlike nanosheets, highly porous, and less porous MoS_2 nanoparticles. Figure 3A–E shows the non-dimensional $i^2/{i_m}^2$ vs. t/t_m curves generated from the CA data for MoS_2 deposition, which reflect the theoretically fitted instantaneous and progressive data of nucleation. At the beginning of current growth, a portion of the non-dimensional graph revealed progressive nucleation at −0.9 V, −1.0 V, and −1.2 V, while a mixed type of instantaneous–progressive nucleation was seen at −1.1 V, respectively. Similarly, at the peak of current growth, the non-dimensional plot revealed progressive (−0.9 V), progressive–instantaneous (−1.0 V), instantaneous (−1.1 V), and progressive–instantaneous processes (−1.2 V), corresponding to

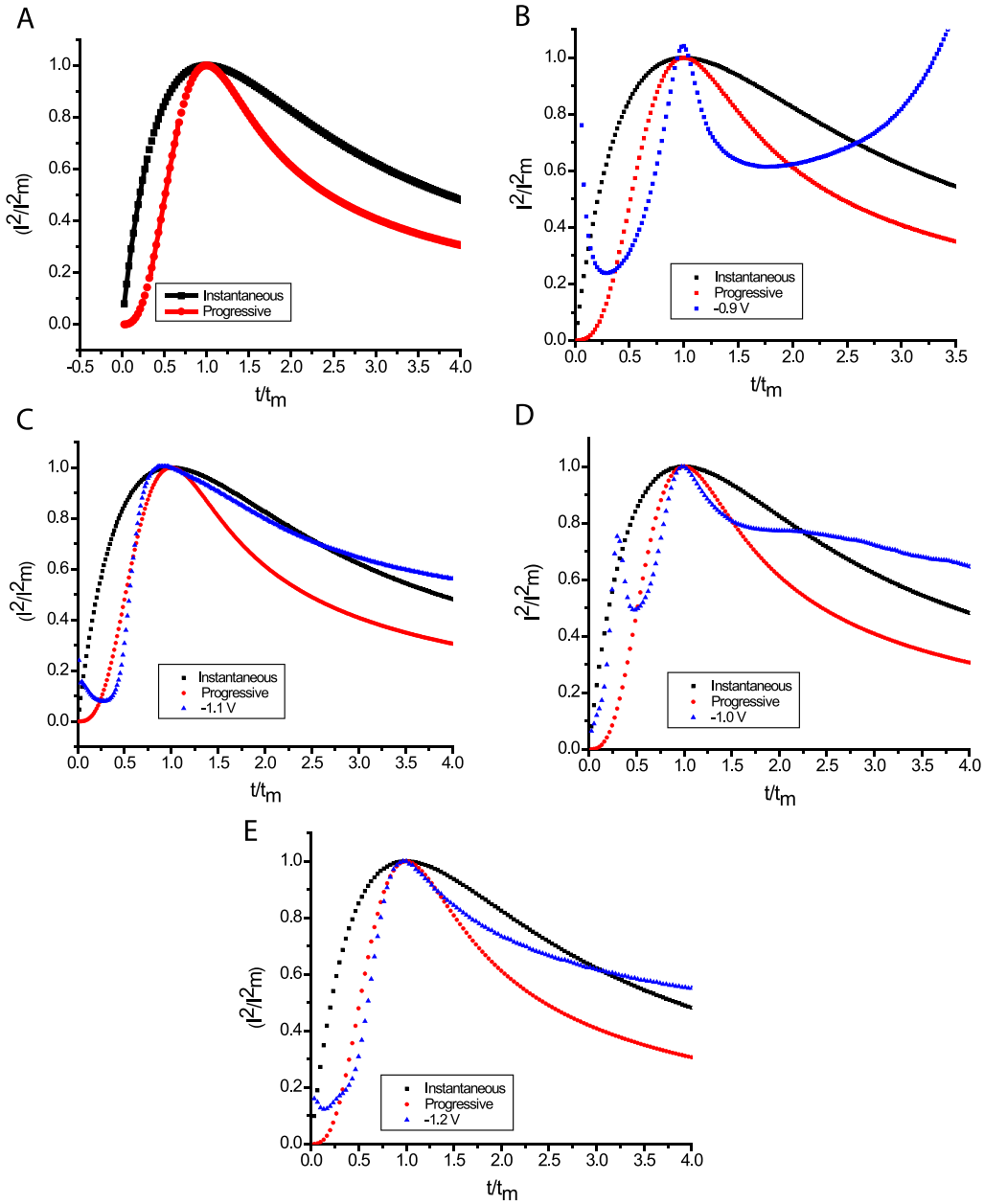

Fig. 3 **A** Theoretical 3D dimensionless time vs. dimensionless current instantaneous and progressive nucleation. **B**–**E** Comparison of 3D dimensionless time vs. dimensionless current (Eq. (1) and (2)) in $Na_2MoO_4.2H_2O$ and $Na_2S.XH_2O$ electrolyte solution and fitted experimental data obtained **B** at −0.9 V **C** at −1.0 V, **D** at −1.1 V, and **E** at −1.2 V vs. the saturated Ag/AgCl electrode based on the Scharifker and Hills (S–H) nucleation model

the SH model. Both the current–time rise and the highest section of the CA data from −0.9 to −1.2 V showed a 3D progressive followed by an instantaneous–progressive pattern. The findings given here provide compelling experimental data, corroborated by SEM morphology acquired under the aforementioned electrodeposition settings, demonstrating that MoS_2 is primarily formed via a 3D progressive followed by immediate nucleation and growth process.

Current–time curves for instantaneous nucleation, diffusion coefficient (*D*) and island density (N_0)

As per the rate law for instantaneous nucleation ($N_{(t)}=N_0$) and diffusion-limited growth, the current maximum and the time at the current maximum can be

determined by the equation provided below. At the current maximum, the instantaneous nucleation growth model is followed.

$$t_m = 1.2564(\pi DN_0)^{-1}c^{-1/2}(8\pi V_m)^{-1/2} \quad (6)$$

$$i_m = 0.6382zFDc^{5/4}(8\pi V_m)^{1/4}(N_0)^{1/2} \quad (7)$$

The parameters i_m and t_m typically exhibit exponential dependencies on the potential, with i_m increasing and tm decreasing as the potential shifts to more negative values. The island density N_0 can be obtained by combining Eqs. (6) and (7):

$$N_0 = 0.065(1/8\pi c_0 V_m)^{1/2}(zFc_0/i_m t_m)^2 \quad (8)$$

The MoS_2 nucleation island density N_0 could be estimated using Eq. (5). Table 1 displays the computed N0 values at −0.9 V, −1.0 V, −1.1 V, and −1.2 V, which are 7.89×10^{10}, 1.02×10^{13}, 1.86×10^{15}, and 3.69×10^{11}, respectively. At −1.1 V, a greater magnitude island density is achieved because progressive and immediate nucleation behaviour is observed at the present growing component. Lower N_0 values at −0.9 V, −1.0 V, and −1.2 V, on the other hand, might be attributed to progressive nucleation in the early stage as well as mixed types of progressive–instantaneous nucleation at the present growing region of the *i*–*t* curve, hence reducing island density. This discovery is compatible with the SEM morphology shown in Fig. 4A–D, respectively. Extracting the diffusion coefficient of the deposited species provides additional verification of the growth process. According to the model for instantaneous nucleation, the diffusion coefficient is linked to the current maximum and the time at the maximum, as seen below (Saravanan and Mohan 2020).

$$D = i_m^2 t_m/0.1629(zFC_0)^2 \quad (9)$$

The given diffusion coefficient $D_0 = 8.5\times10^{-5}$ cm^2 s^{-1} indicates the rate at which ions diffuse in the solution. Since it is relatively high, it suggests that the ions are moving quite rapidly despite the low concentration of 1 M of $Na_2MoO_4{\cdot}2H_2O$.

Current–time curves for progressive nucleation, diffusion coefficient (*D*) and nucleation rate (k_nN_0)

Progressive followed by instantaneous nucleation ($N_{(t)} = k_nN_0$) and diffusion-controlled growth, the current summit and the time at the current maximum are given by Eqs. (10) and (11).

$$i_m = 0.4959zFD^{3/4}C^{9/8}(8\pi V_m)^{1/8}(k_nN_0)^{1/4} \quad (10)$$

$$t_m = 3.318D^{-1/2}(8\pi cV_m)^{-1/4}(k_nN_0)^{-1/2} \quad (11)$$

The potential necessity of a set of deposition current transients is primarily administered by the potential need of the nucleation rate k_nN_0. The nucleation rate ($i_{nucl} = dN_{(t)}/dt = k_nN_0$) could be obtained by merging the equations for i_m and t_m for progressive nucleation.

$$k_nN_0 == 0.2898(8\pi c_0 V_m)^{-1/2}(zFc_0)^2/i_m^2 t_m^3 \quad (12)$$

Hence, the nucleation rates for −0.9 V, −1.0 V, −1.1 V, and −1.2 V potentials were computed using Eq. (9). The degrees of the calculated nucleation rates at −0.9 V , −1.0 V, −1.1 V, and −1.2 V are 1.46×10^{10}, 3.29×10^{12}, 5.75×10^{14}, and 1.47×10^{11}, respectively. For progressive and mixed kinds of instantaneous–progressive nucleation, the diffusion coefficient is derived from Eq. (9) and given as Eq. (13).

$$D = i_m^2 t_m/0.2598(zFc_0)^2 \quad (13)$$

To determine the process of nucleation, compare the two extreme nucleation current transient data at the early stage and at the current maxima of electrochemical deposition for instantaneous and progressive models, as shown in (14) and (15).

$$I_{(t)} = zFD^{1/2}C/\pi^{1/2}t^{1/2}[1 - \exp(-N\pi kDt)] \quad (14)$$

$$I_{(t)} = zFD^{1/2}C/\pi^{1/2}t^{1/2}\left[1 - \exp\left(-(-AN_\infty\pi k'Dt^2/2)\right)\right] \quad (15)$$

Table 1 Shows the effect of electrodeposition potential on the nucleation model, nucleation (island) density and nucleation rate the computed N0 values at − 0.9 V, − 1.0 V, − 1.1 V, and − 1.2 V, which are 7.89 x 10^{10}, 1.02 x 10^{13}, 1.86 x 10^{15}, and 3.69 x 10^{11}, respectively

Electrodeposition potential	t_m (s)	I_m (A)	$t_m i_m$	A	N_0	Initial stage Instantaneous (I)/ progressive(P)	Current maximum Instantaneous (I)/ progressive (P)
−0.9	32	4.2×10^{-3}	134.4×10^{-3}	1.46×10^{10}	7.89×10^{10}	P	P
−1.0	18.5	6.38×10^{-4}	118.0×10^{-4}	3.29×10^{12}	1.02×10^{13}	I & P	P & I
−1.1	24.5	3.57×10^{-5}	87.4×10^{-5}	5.75×10^{14}	1.86×10^{15}	P	I
−1.2	15	4.19×10^{-3}	62.8×10^{-3}	1.47×10^{11}	3.69×10^{11}	P	P & I

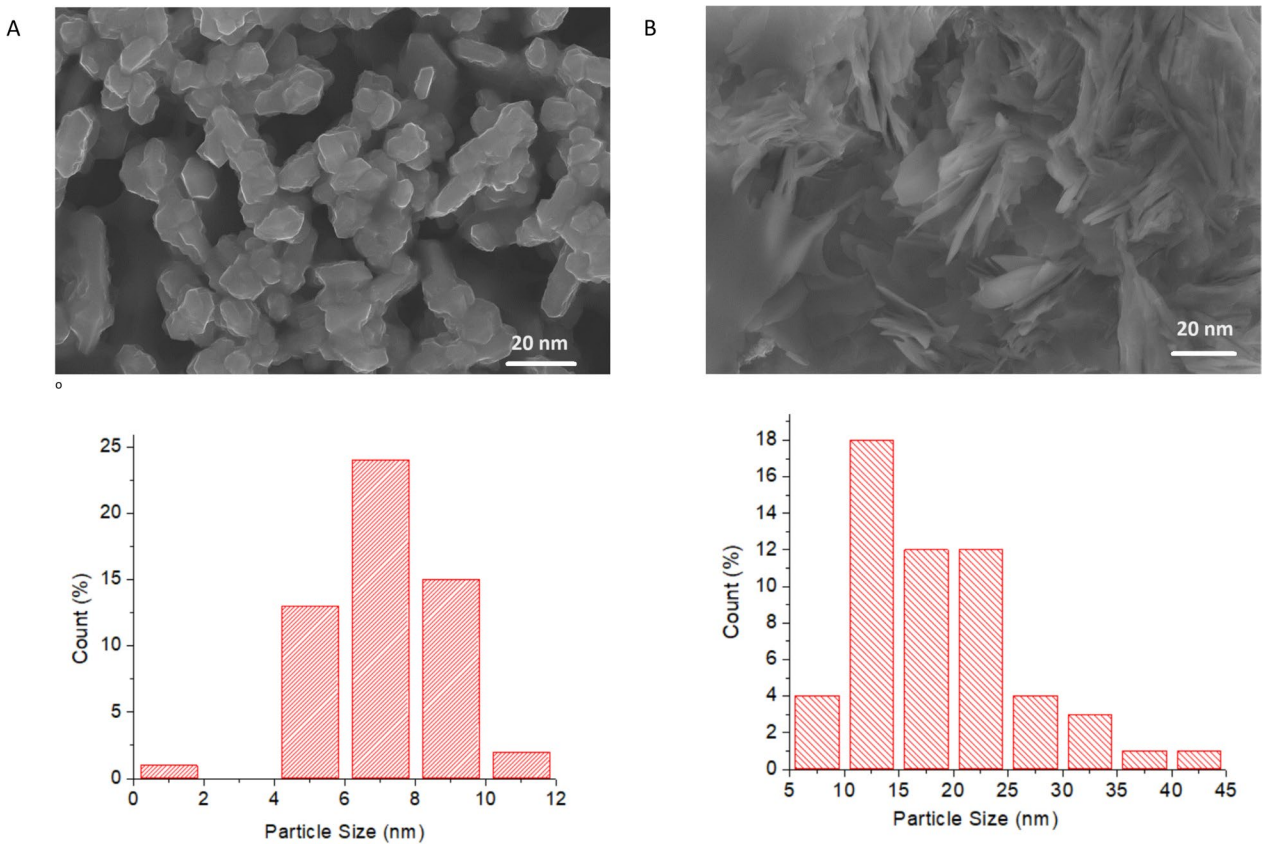

Fig. 4 A–**D** SEM morphologies of electrodeposited fine nodular $FNMoS_2$/Cu, small sheet $SSMoS_2$/Cu, highly porous $HPMoS_2$/Cu, and low porous $LPMoS_2$/Cu at −0.9, −1.0, −1.1, and −1.2 V, respectively, corresponding histogram of particle size distribution

Referring to the formulas, *i(t)* is the current density, t is time, z is the valency of Mo ion, *F* is Faraday's constant, *D* is the diffusion coefficient, *C* is the bulk concentration of Mo ion, and *k* and *k'* are arithmetic constants determined by unique experimental conditions. A indicates the steady-state nucleation rate per site, while N_∞ represents the active site density.

It seems like you are referring to a mathematical derivation involving electrochemical deposition. Equation (4) probably represents the original expression, while Eq. (16) is the simplified form obtained when a certain condition holds, as described by, $N\pi kDt << 1$. This condition implies that the product of $1-\exp(-N\pi kDt) = N\pi kDt$ is much smaller than 1, leading to a simplification of the expression.

$$I_{(t)} = zFD^{3/2}C\pi^{1/2}Nkt^{1/2} \tag{16}$$

And similarly, since $1-\exp(-AN_\infty \pi k'Dt^2/2) = AN_\infty \pi k' Dt^2/2$ Eq. (17) becomes

$$I_{(t)} = \frac{1}{2}zFD^{3/2}C\pi\frac{1}{2}AN_\infty k't^{3/2} \tag{17}$$

Equations (16) and (17) indicate that the plots of *I* versus $t^{1/2}$ for instantaneous nucleation and *I* versus $t^{3/2}$ for progressive nucleation should exhibit linearity, as demonstrated in Fig. 5A and B. Moreover, further expressions can be derived to relate I^2_{max} t_{max} to the diffusion coefficient of electroactive metal ions, as described by the following equations (Wojtalik et al. 2020).

For instantaneous nucleation, i^2_{max} x $t_{max} = 0.1629$ *(zFC)2D,* and for progressive nucleation, it is i^2_{max} x $t_{max} = 0.2598(zFC)2D$. Since the terms on the right-hand side of these equations are independent of applied potential, as per the Scharifker–Hill model, I^2_{max} x t_{max} must be unaffected by the applied potential. Table 1 provides the values of I_{max} t_{max} and I^2_{max} x t_{max} for various overpotentials (Budevski et al. 1996).

Effect of deposition potential and morphology

The surface morphologies of MoS_2 were analysed using transmission electron microscopy (TEM), as depicted in Fig. 6. The impact of deposition potential on the morphology of $FNMoS_2$, $SSMoS_2$, $HPMoS_2$, and $LPMoS_2$ was investigated through TEM. The results revealed that the deposition potential primarily influences the density of

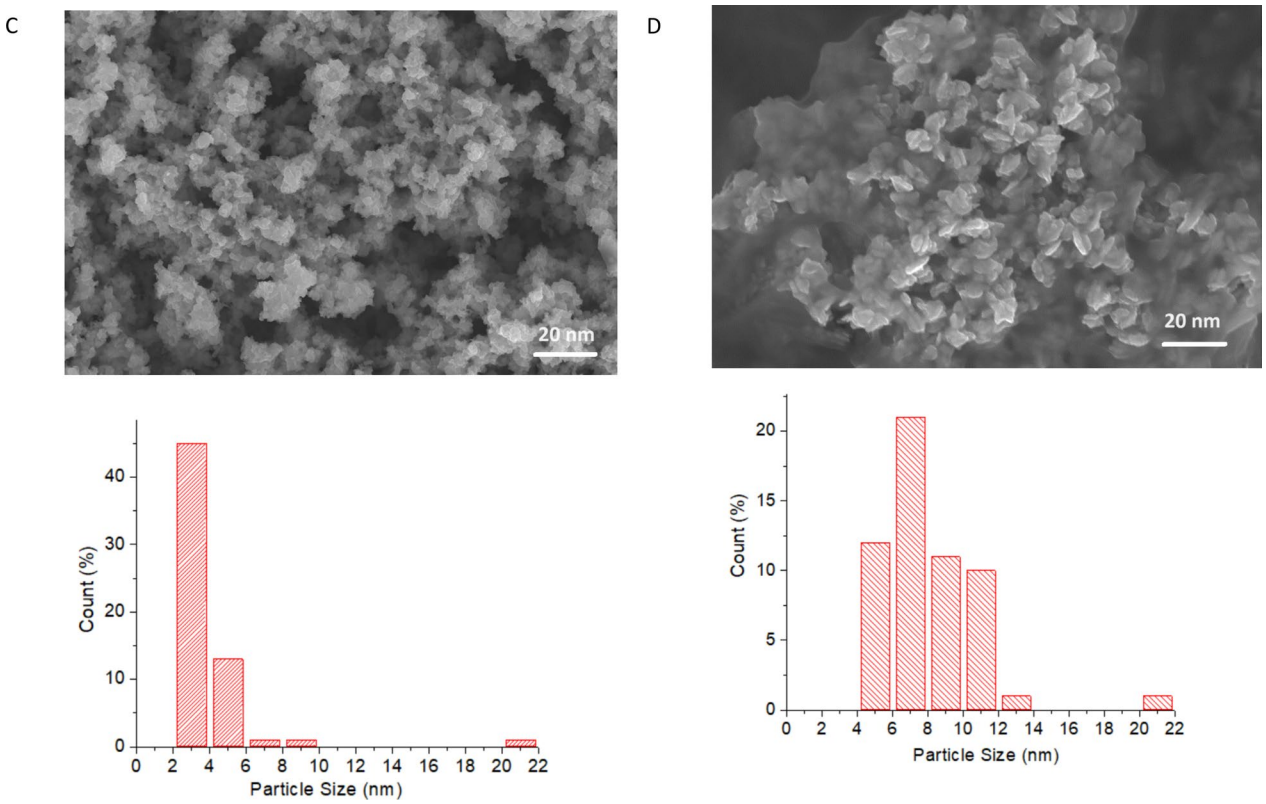

Fig. 4 continued

MoS_2 nuclei within the range of −0.9 V, −1.0 V, −1.1 V, and −1.2 V. Figure 6A–D shows that the fine nodular nuclei were smaller, with small sheetlike morphology and highly porous small nuclei, with nucleation island density N_0 calculated value (Table 1), consistent with TEM images. The measured population density increases with increasing deposition potential from −0.9 to −1.1 V, from 7.89×10^{10}, 1.86×10^{15} and then started to decrease to 3.69×10^{11}. The rise in population density at higher deposition potential can be attributed to the shift from progressive to instantaneous nucleation growth. This transition involves the formation of new nuclei alongside existing ones. Conversely, the decrease observed at higher overpotential may be linked to progressive nucleation occurring in both the initial and current growing parts of the cathodic area. Therefore, the overall total nucleation density increased. The TEM images of $FNMoS_2$, $SSMoS_2$, $HPMoS_2$, and $LPMoS_2$ also support the calculated nucleation density(N_0) and nucleation rate (A) and the average sizes are 6–8 ± 1.5 nm, 10–25 ± 2 nm, 2–4 ± 1.3 nm and 6–8 ± 1.5 nm, respectively.

From the high-resolution transmission electron microscopy (HRTEM) image of the 1 T phase of $HPMoS_2$, a trigonal lattice with octahedral coordination is displayed, showing an intersheet spacing of 0.634 nm, which may be attributed to intercalated Na^+ ions. On the other hand, the samples of $FNMoS_2$/Cu, $SSMoS_2$/Cu, and $LPMoS_2$/Cu exhibit a honeycomb hexagonal lattice, characteristic of the 2H phase. This lattice consists of 3 Mo atoms and 3 overlapped S atoms. This discussion prompts an examination of the interplanar spacing of the (002) plane in relation to electrodeposited $HPMoS_2$ at −1.1 V, which predominantly forms the 1 T phase with a larger interplanar d-spacing. Other electrodeposited materials, such as $FNMoS_2$, $SSMoS_2$, and $LPMoS_2$, mostly adopt the 2H phase, exhibiting smaller d-spacings than those observed in $HPMoS_2$. Figure 7 illustrates the evaluation of the hydrogen evolution reaction (HER) process via linear sweep voltammetry (LSV) studies. These studies were performed with a sweep rate of 5 mV s^{-1}, covering a potential range from −0.8 to 0.5 V. Notably, the $HPMoS_2$/Cu-modified electrode exhibited a significant cathodic current in the small overpotential region, achieving an onset potential of −287 mV at a current density of 10 mA/cm^2. This result is similar to the performance of Pt/C 20%, to a certain extent. Furthermore, $FNMoS_2$/Cu, $SSMoS_2$/Cu, and $LPMoS_2$/Cu have demonstrated improved HER performance, achieving onset potentials of −305 mV, −327 mV, and −332 mV, respectively. To elaborate, the 1 T phase of the $HPMoS_2$/Cu electrocatalyst possesses an expanded d-spacing and highly

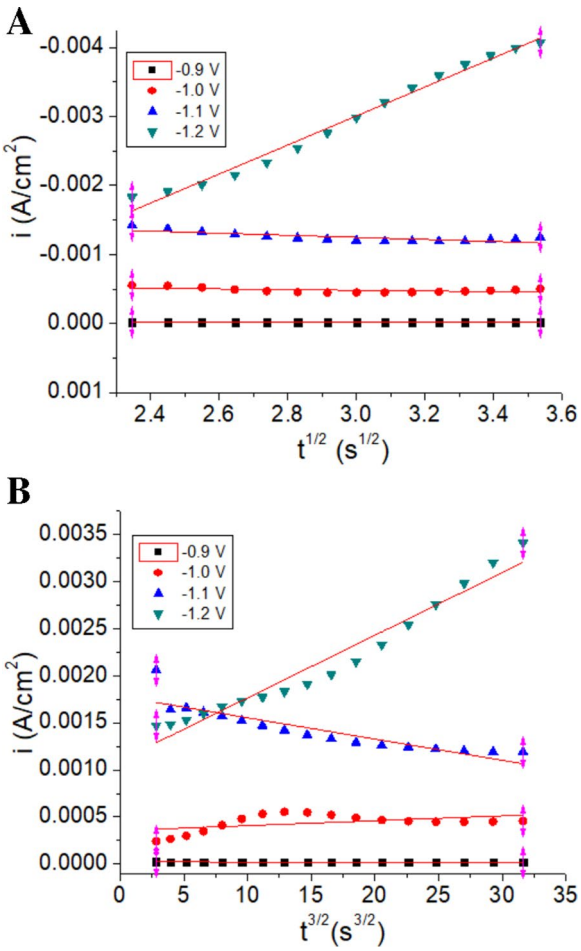

Fig. 5 **A** Plot of early stage of current transient curves for electrochemical phase formation MoS2 on Cu 5A in I vs $t^{1/2}$ and **B** in I vs $t^{3/2}$ which shows curve fitting to experimental data

porous nanostructure, which enhances electron and electrolyte transport, thereby accelerating the electrocatalytic HER process. Tafel plots, which plot log current density against overpotential, provide a quantitative analysis of the electrode kinetics of the HER process. To enhance comprehension of the HER catalytic mechanism in KOH medium, a detailed explanation of the three principal steps that have been proposed and are involved in this process is required.

$$2H_2O + 2e^- \rightarrow H^+_{2(g)}2OH^-_{(aq)}$$

$$2H_2O + 2e^- \rightarrow 2H_{ads} + 2OH^- \text{(Water dissociation in Volmer step; 120 mV/dec)}$$

$$2H_{ads} \rightarrow H_{2(g)} \text{(Tafel step; 30 mV/dec)}$$

$$H_{ads} + e^- \rightarrow H_2 + OH^- \text{(Heyrovsky step; 120 mV/dec)}.$$

Several strategies have been developed to enhance the performance and reliability of MoS_2 materials for the hydrogen evolution reaction (HER). One such approach involves: (a) augmenting the quantity of exposed active edge sites, as detailed in the literature (Oskam et al. 1998; Xie et al. 2013); (b) improving the electrical conductivity and diffusion of MoS_2 electrocatalysts, as described in references (Ambrosi et al. 2015a; Lukowski et al. 2014; Zhang et al. 2015); and (c) enhancing catalytic activities of active sites through intercalation, as described in reference (Ambrosi et al. 2015b). It is important to note that MoS_2 can exist in two phases: trigonal prismatic 2H and octahedral 1 T. Naturally occurring MoS_2 tends to be semiconducting and thermodynamically favours the 2H phase. However, the 1 T metallic phase can be achieved through exfoliating bulk 2H-MoS_2 chemically or electrochemically. The 2H phase of MoS_2 has limitations, including limited active sites and inadequate electron transfer properties which can limit catalytic performance. In order to enhance the catalytic performance of the 2H phase, it can be electrochemically converted into the 1 T phase, which has been shown to exhibit advanced catalytic activity compared to the 2H phase is attributed to its active edge and basal planes. The exceptional catalytic properties of the 1 T phase of MoS_2 are associated with its high affinity for water. strong electron transport, and ability to interact with various ions. However, to gain a comprehensive understanding of the electrocatalytic nature of 1 T-MoS_2, further investigation is needed into its interfacial properties, electrical conductivity, active sites, and the specific type of hydrogen evolution reaction (HER) mechanism it facilitates. The catalytic activity of basal surfaces can be increased through intercalation processes, which create more active sites such as terraces, kinks, steps, and corner atoms via surface engineering. These active sites have the potential to significantly enhance the catalytic activity of the hydrogen evolution reaction (HER). When a sodium ion is intercalated into $HPMoS_2$ nanosheets, the intersheet d-spacing increases from 0.613 to 0.643 nm. However, it is important to note that only alkali metal ions with appropriate radii can successfully penetrate the interlayer gap distance of $HPMoS_2$. When discussing the hydrogen adsorption sites in the context of the HER, it is important to clarify that the reactant changes depending on whether the medium is acidic or basic. In acidic media, the reactant is hydronium (H_3O^+), while in basic media, the reactant is water (H_2O). During the simple step for the reaction, the H^-_{ads} species appears to be the primary intermediate on the electrode surface.

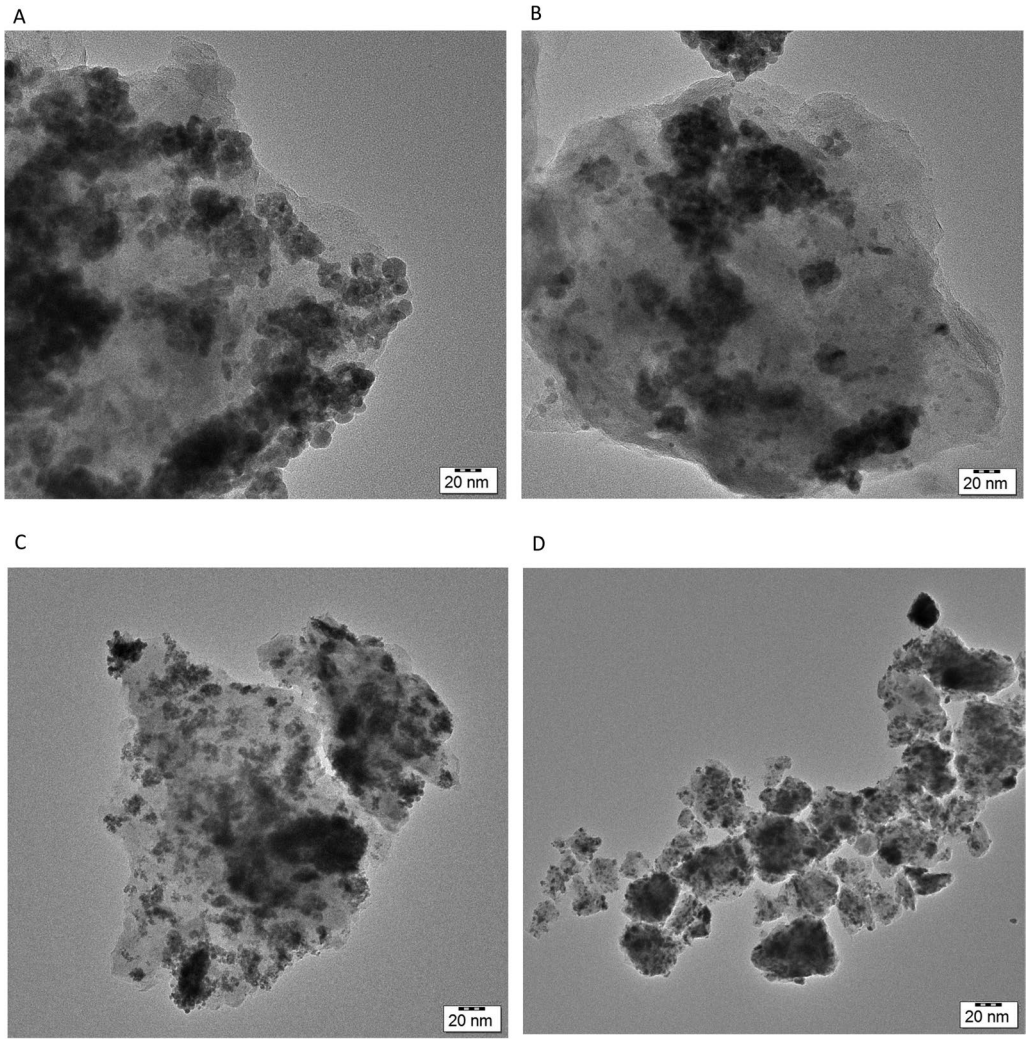

Fig. 6 **A–D** TEM images of electrodeposited $FNMoS_2$/Cu, $SSMoS_2$/Cu, $HPMoS_2$/Cu, and $LPMoS_2$/Cu at −0.9, −1.0, −1.1, and −1.2 V, respectively

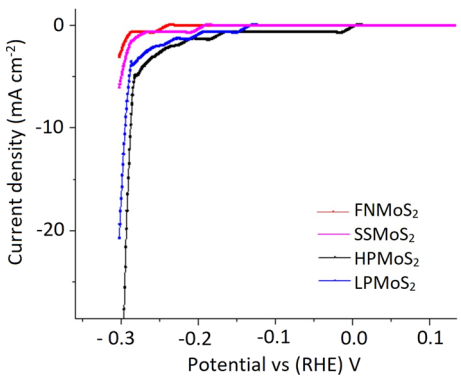

Fig. 7 Representative linear sweep voltammetry (LSV) measurements were taken in 0.5 M KOH with a scan rate of 5 mV s^{-1} over the potential range of −0.8 to 0.5 V for $FNMoS_2$/Cu, $SSMoS_2$/Cu, $HPMoS_2$/Cu, and $LPMoS_2$/Cu at −0.9, −1.0, −1.1, and −1.2 V, respectively

As a result, methods such as surface assimilation and sorption of adsorbed hydrogen (H) atoms become viable options. However, there is competition for these methods in both acidic and basic environments, where anions like Cl^-, $ClO4^-$, and SO_4^{2-} or OH^- can impact the complete hydrogen binding energy quanta. Therefore, achieving the optimal hydrogen binding energy is crucial for maintaining a balance between the adsorption and removal of hydrogen intermediates in basic solutions. The first step of the hydrogen evolution reaction (HER) on the basal sheet of 1 T-$HPMoS_2$ entails the adsorption of a hydrogen atom on the sulphur (S) atom, with a minor barrier of 0.16 eV. This is succeeded by a Heyrovsky step, where the adsorbed hydrogen atom reacts with a proton (H_3O+) to generate H_2, passing through a barrier of 0.62 eV. This indicates that HER occurs readily on the basal sheet of 1 T-$HPMoS_2$ through the Volmer–Tafel mechanism. Previous studies have reported that intercalation of alkali

and alkaline earth ions into the 1 T-MoS_2 intersheet area resulted in a decrease in the overpotential of the HER process.

Conclusions

The combination of electrochemistry with scanning electron microscopy (SEM) proved to be a successful experimental approach for studying the nucleation and growth model of MoS_2 during the initial stages of electrodeposition. Electrochemical techniques served a dual role: (a) facilitating MoS_2 electrodeposition and (b) providing mechanistic interpretation. SEM proved invaluable in linking MoS_2 size distribution with electrochemical observations. Among the parameters explored, it was noted that a transition from progressive nucleation to a mixed instantaneous–progressive nucleation occurred during the initial current growth stage, spanning potentials from -0.9 to -1.2 V. Similarly, during the current growth maximum stage, the non-dimensional plot exhibited a progression from progressive nucleation (-0.9 V) to progressive–instantaneous nucleation (-1.0 V), followed by instantaneous nucleation (-1.1 V), and a mix of progressive–instantaneous mechanism (-1.2 V) according to the Scharifker–Hills (SH) model. Overall, the 3D progressive followed by instantaneous–progressive mechanism was observed both for the increase in current over time and at the maximum part of the chronoamperometric data across the potential range from −0.9 to −1.2 V. The observations presented here provide convincing experimental evidence, supported by SEM morphology, that MoS_2 is predominantly obtained through the 3D progressive followed by instantaneous nucleation and growth mechanism under the mentioned electrodeposition conditions. The MoS_2 nucleation island density (N_0) and nucleation rate (A) values at -0.9 V, -1.0 V, -1.1 V, and -1.2 V are 7.89×10^{10}, 1.02×10^{13}, 1.86×10^{15}, and 3.69×10^{11}, and 1.46×10^{10}, 3.29×10^{12}, 5.75×10^{14}, and 1.47×10^{11}, respectively. A higher magnitude island density is obtained at −1.1 V, attributed to the progressive at initial and instantaneous nucleation behaviour during the current growth phase, which reduces the island density. This observation aligns with the SEM and TEM morphology results. These findings may open up new avenues for developing novel, earth-abundant, low-cost, and highly efficient transition metal dichalcogenide (TMDC)-based electrocatalysts for hydrogen evolution reactions.

Acknowledgements
Saravanan Gengan wishes to express their sincere thanks to the Director, Principal, Dean, SIMATS School of Engineering Chennai, for constant encouragement and support. This work was supported by the Science and Engineering Research Board (SERB) under Core Research Grant (CRG) (CRG/2019/005985)

Author contributions
Venumbaka Maneesh Reddy—Conceptualization, Methodology. Marepally Bhanu Chandra—Funding acquisition, Investigation. Saravanan Gengan—Methodology, Writing-original draft, Visualization. Selvakumar Duraisamy—Supervision, editing draft.

Funding
This work was supported by the Science and Engineering Research Board (SERB) under Core Research Grant (CRG) (CRG/2019/005985).

Availability of data and materials
All the data are available in our attachment files like manuscript, figures, and table.

Declarations

Ethics approval and consent to participate
1. All experiments were performed in compliance with relevant laws/guidelines. 2. The experiments followed institutional guidelines. 3. The relevant institutional committee approved the experiments. 4. Informed consent was obtained.

Competing interests
The authors declare no competing financial interest.

Received: 10 September 2024 Accepted: 28 October 2024
Published online: 02 December 2024

References

Alinejadian N, Kollo L, Odnevall I. Progress in additive manufacturing of MoS_2-based structures for energy storage applications: a review. Mater Sci Semicond Process. 2022;139:106331.
Ambrosi A, Sofer Z, Pumera M. Lithium intercalation compound dramatically influences the electrochemical properties of exfoliated MoS_2. Small. 2015a;11:605–12.
Ambrosi A, Sofer Z, Pumera M. 2H → 1T phase transition and hydrogen evolution activity of MoS2, MoSe2, WS_2 and WSe_2 strongly depends on the MX_2 composition. Chem Commun. 2015b;51:8450–3.
Aslan E, Yanalak G, Patir IH. Enhanced hydrogen evolution reaction catalysis at template-free liquid/liquid interfaces by in situ electrodeposited amorphous molybdenum sulfide on carbon nanotubes. ACS Appl Energy Mater. 2021;4(8):8330.
Budevski E, Staikov G, Lorenz WJ. Electrochemical phase formation and growth. New York: VCH Verlagsgesellschaft mbH; 1996.
Cottrell FGZ. Der Reststrom bei galvanischer Polarisation, betrachtet alsein Diffusionsproblem. J Phys Chem. 1903;42:385–431.
Du Y, Yang L, Zhou Y, Wu JZ, Fu W, Dumas DC, Jiang Y. Pre-lithiation of onion-like carbon/MoS_2 nano-urchin anodes for high-performance rechargeable lithium-ion batteries. Nanoscale. 2014;6:8488.
Gunawardena G, Hills G, Montenegro I, Scharifer B. Electrochemical nucleation: part I. General considerations. J Electroanal Chem. 1982;138:225–39.
Kong D, Wang H, Lu Z, Cui Y. $CoSe_2$ nanoparticles grown on carbon fiber paper: an efficient and stable electrocatalyst for hydrogen evolution reaction. J Am Chem Soc. 2014;136:4897.
Lembke D, Kis A. Breakdown of high-performance monolayer MoS_2 transistors. ACS Nano. 2012;6:10070.
Li H, Wu J, Yin Z, Zhang H. Preparation and applications of mechanically exfoliated single-layer and multilayer MoS_2 and WSe_2 nanosheets. Acc Chem Res. 2014;47:1067.
Lukowski MA, Daniel AS, English CR, Meng F, Forticaux A, Hamers RJ, Jin S. Highly active hydrogen evolution catalysis from metallic WS_2 nanosheets. Energy Environ Sci. 2014;7:2608–13.
Mak KF, Lee C, Hone J, Shan J, Heinz TF. Atomically thin MoS_2: a new direct-gap semiconductor. Phys Rev Lett. 2010;105:136805.

Novoselov KS, Jiang D, Schedin F, Booth TJ, Khotkevich VV, Morozov SV, Geim AK. Two-dimensional atomic crystals. Proc Natl Acad Sci USA. 2005;102:10451.
Oskam G, Long JG, Natarajan A, Searson PC. Electrochemical deposition of metals onto silicon. J Phys D Appl Phys. 1998;31:1927.
Radisavljevic B, Radenovic A, Brivio J, Giacometti V, Kis A. Single-layer MoS_2 transistors. Nat Nanotechnol. 2011;6:147.
Saravanan G, Mohan S. Pt nanoparticles embedded on reduced graphite oxide with excellent electrocatalytic properties. Appl Surf Sci. 2016;386:96–102.
Saravanan G, Mohan S. Electrochemical nucleation and growth of Pt nanoflower particles on reduced graphite oxide with electrooxidation of glucose. Anal Methods. 2020;12:3617–25.
Scharifer B, Hills G. Theoretical and experimental studies of multiple nucleation. Electrochim Acta. 1983;28:879–89.
Shi Y, Zhou W, Xu A, Guo S, Zhang J, Wu Y, Li H, Zhang H, Xie Y. Graphene oxide: a promising nanomaterial for energy and environmental applications. Nano Energy. 2012;1:214.
Shi Y, Wang J, Zhang J, Ma X, Zhang L, Yang X. Electrocatalytic hydrogen evolution under alkaline conditions: current state and perspectives. Chem Soc Rev. 2015;44:886.
Singh AW, Jain M, Bhumla P, Bhattacharya S. Electrocatalytic study of the hydrogen evolution reaction on MoS_2/BP and MoSSe/BP in acidic media. Nanoscale Adv. 2023;5:5332.
Splendiani A, Sun L, Zhang Y, Li T, Kim J, Chim C-Y, Galli G, Wang F. Emerging photoluminescence in monolayer MoS_2. Nano Lett. 2010;10:1271.
Tan C, Zhang H. Wet-chemical synthesis and applications of non-layer structured two-dimensional nanomaterials. Nat Commun. 2015;6:7873.
Voiry D, Fullon R, Yang J, Santos I, Zhang J, Li L, Chhowalla M. The role of electronic coupling between substrate and 2D MoS_2 nanosheets in electrocatalytic production of hydrogen. Nat Mater. 2016;15:1003.
Wang H, Tsai C, Kong D, Chan K, Abild-Pedersen F, Nørskov JK, Cui Y. Transition-metal doped edge sites in vertically aligned MoS_2 catalysts for enhanced hydrogen evolution. Nano Res. 2015;8:566–75.
Wojtalik M, Orciuch W, Makowski Ł. Nucleation and growth kinetics of MoS_2 nanoparticles obtained by chemical wet synthesis in a jet reactor. Chem Eng Sci. 2020;225:115814.
Xie J, Zhang H, Li S, Wang R, Sun X, Zhou M, Zhou J, Lou XW, Xie Y. Defect-rich MoS_2 ultrathin nanosheets with additional active edge sites for enhanced electrocatalytic hydrogen evolution. Adv Mater. 2013;25:5807–13.
Yin Z, Li H, Li H, Jiang L, Shi Y, Sun Y, Lu G, Zhang Q, Chen X, Zhang H. Single-layer MoS_2 phototransistors. ACS Nano. 2012;6:74.
Yu Y, Li C, Liu Y, Su L, Zhang Y, Cao L. Controlled scalable synthesis of uniform, high-quality monolayer and few-layer MoS_2 films. Sci Rep. 2013;3:1866.
Yu Y, Huang S, Li Y, Steinmann S, Yang W, Cao L. Layer-dependent electrocatalysis of MoS_2 for hydrogen evolution. Nano Lett. 2014;14:553.
Zeng M, Xiao Y, Liu J, Yang K, Fu G, Shen Z, Fu L. An artificial solid electrolyte interphase with high li-ion conductivity, mechanical strength, and flexibility for stable lithium metal anodes. Adv Mater. 2017;29:1703358.
Zhang Z, Li W, Yuen MF, Ng TW, Tang Y, Lee CS, Chen X, Zhang W. Hierarchical composite structure of few-layers MoS_2 nanosheets supported by vertical graphene on carbon cloth for high-performance hydrogen evolution reaction. Nano Energy. 2015;18:196–204.
Zhou W, Zou X, Najmaei L, Liu Z, Shi Y, Kong J, Lou A, Ajayan P, Lou J, Yakobson BI, Idrobo JC. Intrinsic structural defects in monolayer molybdenum disulfide. Nano Lett. 2013;13:2615.

Publisher's Note